Available online at www.CivileJournal.org

Civil Engineering Journal

(E-ISSN: 2476-3055; ISSN: 2676-6957)

Vol. 12, No. 02, February, 2026

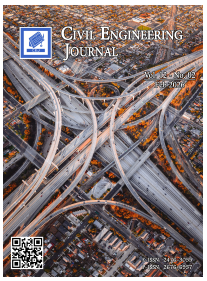

Functional Verification of a Stainless Steel Reference Block for Calibration of Industrial Ultrasonic Test System

Jorge Vera [1*], Luis Caballero [2], Martín Taboada [1], Luis Aguilar [1], Braulio Briceño [1], Eduardo Azabache [3]

[1] *School of Metallurgical Engineering, Universidad Nacional de Trujillo, Trujillo 13001, Peru.*

[2] *Faculty of Engineering, Universidad Tecnológica del Perú, Trujillo 13001, Peru.*

[3] *School of Mechanical Engineering, Universidad Nacional de Trujillo, Trujillo 13001, Peru.*

Received 11 November 2025; Revised 17 January 2026; Accepted 21 January 2026; Published 01 February 2026

Abstract

In the construction and assembly of metal structures, ultrasonic testing constitutes a pillar for the guarantee of structural integrity. This study aimed to develop and experimentally validate a semi-cylindrical reference block, optimized for the ultrasonic inspection of welds in austenitic stainless steels under the AWS D1.6 code. Unlike conventional devices, this proposal integrates three functional zones into a unified body. Methodologically, the acoustic properties of velocity and attenuation coefficient were characterized using the pulse-echo technique with 2.25 and 5.0 MHz transducers, validating the results through analysis of variance (ANOVA) and Pearson correlation. The findings revealed a statistically significant influence of frequency on the acoustic properties of the material. Functionally, experimental tests demonstrated that the geometric arrangement of three integrated references allows for the efficient construction of Distance-Amplitude Correction (DAC) curves and direct angular verification, overcoming the logistical limitations of conventional prismatic blocks. The main novelty of the device lies in its capacity to unify the functions of sensitivity, resolution, and distance calibration into a single body of acoustically equivalent material, eliminating the need for complex correction factors and ensuring greater precision in industrial inspection.

Keywords: Quality; Stainless Steels; Innovation; NDT.

1. Introduction

In the construction and metalworking industries, the structural integrity of welded joints is a fundamental requirement for ensuring the safety and operability of infrastructure. Among Non-Destructive Testing (NDT) methods, Ultrasonic Testing (UT) has established itself as a standard technique due to its high sensitivity for detecting internal discontinuities without compromising the integrity of the tested component [1, 2]. However, the reliability of these examinations is inherently dependent on the precise calibration of the inspection system, a process that necessitates the use of standardized reference blocks to verify the linearity, sensitivity, and resolution [3].

Metallic materials have established themselves as fundamental elements in diverse engineering applications due to their versatility, high mechanical strength, and durability [4, 5]. In particular, stainless steels play a critical role in both modern construction—in beams, columns, and reinforcements—and the industrial sector for the manufacturing of tanks

* Corresponding author: jvera@unitru.edu.pe

https://doi.org/10.28991/CEJ-2026-012-02-09

and pressure vessels [6]. Given the severity of their service conditions, these infrastructures demand rigorous safety standards to mitigate the risk of failure and extend their service life. In this context, Non-Destructive Testing (NDT) constitutes an indispensable tool for the early detection of defects and the assurance of structural integrity [6–8].

Recent investigations have evaluated the efficacy of ultrasonic methods both for the detection of discontinuities in stainless steel welded joints [9–11] and for the acoustic characterization of microstructural changes [12]. Welded joints constitute the zones most susceptible to defect formation due to phase transformations induced by the thermal cycles of the welding process. Consequently, quality assurance is critically focused on these regions, the typical defects of which are detailed in [13]. For the evaluation of internal or 'volumetric' defects, the use of deep penetration inspection techniques is required. In this context, ultrasonic testing is distinguished by its high capability to detect internal discontinuities, measure thickness, and monitor corrosion, serving as a superior alternative in stainless steels where radiography presents limitations regarding contrast or detection [14, 15].

It is widely recognized that the reliability of the ultrasonic testing system and the accuracy of defect localization depend inherently on rigorous calibration [16]. This process is typically performed using reference blocks standardized by bodies such as the American Welding Society (AWS). However, the inspection of austenitic stainless steels, governed by the AWS D1.6 code [3], poses unique acoustic challenges. The microstructure of these materials, characterized by coarse grains and a dendritic morphology, induces severe phenomena of anisotropy, scattering, and attenuation that compromise detection if not adequately compensated for [17, 18]. In this context, conventional blocks (Type IIW or DSC), although optimal for carbon steel, present operational limitations: they tend to be bulky and of restricted functionality. This requires the inspector to transport multiple standards to construct a complete Distance-Amplitude Correction (DAC) curve, thereby complicating field logistics [19].

Section 8 of the AWS D1.6 code [3] establishes the requirements for pulse-echo inspection, mandating the construction of a Distance-Amplitude Correction (DAC) curve. This reference compensates for energy losses due to beam divergence and attenuation, ensuring uniform sensitivity along the beam path to precisely size and locate defects [16, 20]. During evaluation (Figure 1), indications are classified by comparing their amplitude against regulatory limits: the Standard Sensitivity Level (SSL) and the Disregard Level (DRL, -6 dB) [3, 21]. The rigor of this calibration is critical in metallic materials, where attenuation is not constant but is dependent on scattering caused by grain size and the microstructural complexity of the polycrystalline medium [22–28].

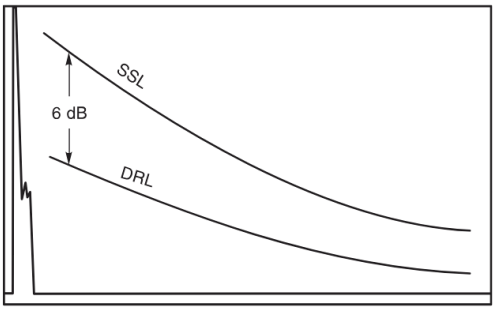

Figure 1. DAC curve and discontinuity amplitude levels [3]

An analysis of recent literature reveals a growing interest in optimizing calibration standards. Various studies have reviewed the expansion of ultrasonic testing in the evaluation of civil infrastructure, underscoring the need for more versatile standards [29]. Furthermore, current trends prioritize the use of Finite Element Method (FEM) simulations to predict wave propagation [30-32], and additive manufacturing, driving innovations in reference block design [33, 34].

However, despite these technological advances, the inspection of stainless-steel welds continues to face critical challenges regarding anisotropy and acoustic equivalence, which demand more robust solutions [35, 36]. Current studies, such as those by Rawicki et al. [17] and Li et al. [37], have documented that the columnar grain structure induces severe beam skewing, which hinders the precise determination of the refraction angle on flat surfaces. In this context, a significant technological gap is identified: the absence of 'all-in-one' devices that integrate multiple volumetric references (angular, sensitivity, and resolution) into a compact geometry.

To address this deficiency and mitigate logistical issues under AWS regulations, the present research proposes a semi-cylindrical calibration block, based on the design criteria of the UNT patent [38], The geometric configuration of the block is strictly grounded in the limitations reported by recent literature regarding the inspection of austenitic stainless steels. The semi-cylindrical geometry, as shown in Figure 2, unlike prismatic blocks, ensures normal incidence of the reflected beam toward the transducer. This enables the validation of 45°, 60°, and 70° angles through the maximization of backwall echoes, an effective method for reducing uncertainty in

anisotropic media [39]. Furthermore, given that attenuation in coarse-grained materials is dominated by nonlinear stochastic scattering [18], a series of three stepped side-drilled holes (SDH) was incorporated. This arrangement enables the inspector to construct multipoint correction curves, accurately capturing the material's amplitude loss [40]. Finally, in accordance with the criteria of Krautkrämer & Krautkrämer [41] and the AWS D1.6 standard [3], the block dimensions ensure that all reflectors are located within the far-field zone (Fraunhofer), guaranteeing stable and repeatable readings.

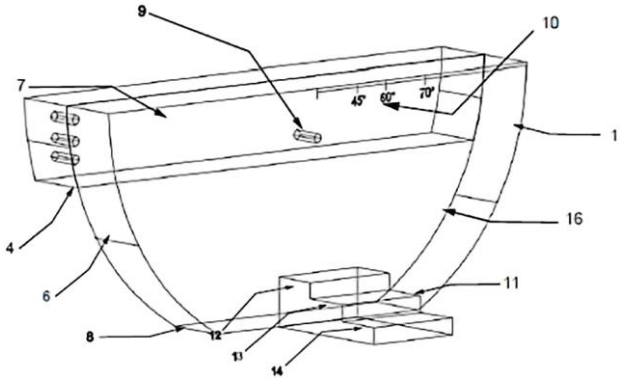

Figure 2. Geometric details of the reference block [38]

This device is distinguished by integrating three reference zones into a single body, facilitating the generation of both longitudinal and shear waves. The design of the block's second reference (angular scale) is grounded in the theory of elastic wave refraction. To generate the shear (transverse) waves required for weld inspection according to AWS D1.6 [3], the block leverages the change in acoustic velocity at the wedge-steel interface. The angle of refraction Θ_2 is determined according to Equation 1 [41], using the generalized Snell's Law, where Θ_1 is the angle of incidence, $V_L^{(1)}$ is the longitudinal velocity in the wedge (plexiglass), and $V_S^{(2)}$ is the shear velocity in the steel block. The semi-cylindrical geometry allows for the verification of these angles (45°, 60°, 70°) by ensuring that the sound beam achieves normal incidence upon the curved surface, thereby maximizing the energy reflected back to the transducer.

$$\frac{sin\,\theta_1}{V_L^{(1)}} = \frac{sin\,\theta_2}{V_S^{(2)}} \tag{1}$$

The block's first reference zone employs Side-Drilled Holes (SDH). Theoretically, an SDH functions as an ideal cylindrical reflector that scatters the incident wave uniformly across all radial directions. The reflected acoustic pressure (Pr) from an SDH is theoretically modeled as specified in Equation 2 [41], where Pi is the incident pressure, r is the hole radius, and z is the distance. This theoretical relationship justifies the use of holes of identical diameter positioned at varying depths to construct the DAC curve, as distance (encompassing attenuation and beam divergence) remains the sole dependent variable, thereby eliminating geometric factors associated with the reflector.

$$P_r = P_i\sqrt{\frac{r}{z}} \tag{2}$$

The physical sizing of the block was theoretically calculated to avoid measurements within the near field (Fresnel zone), where acoustic pressure is unstable due to wave interference. The near-field length (N) is theoretically defined according to Equation 3, [41] where D is the transducer diameter and λ is the wavelength in the material. The dimensions of the three volumetric references ensure that calibrations are performed within the Fraunhofer zone (far field), guaranteeing a linear and predictable response.

$$N = \frac{D^2}{4\lambda} \tag{3}$$

From an operational perspective, the construction of Distance-Amplitude Correction (DAC) curves using conventional prismatic blocks proves inefficient, requiring multiple standards and handling steps that increase the likelihood of human error. Against this background, the central motivation of this work was to develop a unified reference geometry that not only guarantees the acoustic similarity required by AWS regulations but also optimizes logistics through an integral design. Consequently, the objective of the research was the development and validation of a semi-cylindrical calibration block that integrates three volumetric references into a single device. The remainder of the article is structured as follows: Section 1 details the design and theoretical foundations; Section 2 describes the experimental methodology; Section 3 presents the results and discussion; and Section 4 outlines the conclusions.

2. Materials and Methods

2.1. Study Material

The reference block was fabricated from a solid bar of structural-grade AISI 304 austenitic stainless steel, with a nominal diameter of 165.10 mm. The chemical composition, certified by the manufacturer, reported a content of 15.24% Cr, 8.26% Ni, 1.95% Mn, 0.363% Si, 0.04% C, and 0.03% P. To ensure microstructural stability, the base material was subjected to solution annealing at 1080 °C for 90 minutes, followed by water quenching. The geometric profile was achieved through precision machining, adhering to the design criteria of the UNT patent [38] and ensuring a polished surface finish with strict parallelism between faces. Dimensional verification was performed using digital metrology with a resolution of 10 µm. Given the device's purpose as a calibration standard, destructive metallographic sectioning was omitted; instead, material homogeneity was validated through acoustic uniformity characterization, following the guidelines of the ASTM E1065 standard [42].

Figure 3 illustrates that the block possesses a semi-cylindrical geometry distinctly divided into three calibration references. The first reference, due to its geometry, is optimal for distance calibration using longitudinal waves. Furthermore, it incorporates three artificially introduced holes of 1.6 mm in diameter, which enabled the establishment of the DAC curve. The second reference facilitated distance calibration with both longitudinal and shear waves. Additionally, aided by its 1.6 mm diameter hole and an angular scale in sexagesimal (0°, 45°, 60° y 70°), it allowed for sensitivity evaluation and the verification of the refraction angle. The third reference features three steps with decreasing thicknesses, which are useful for distance calibration using longitudinal beams and for subsequent inspection for thickness verification.

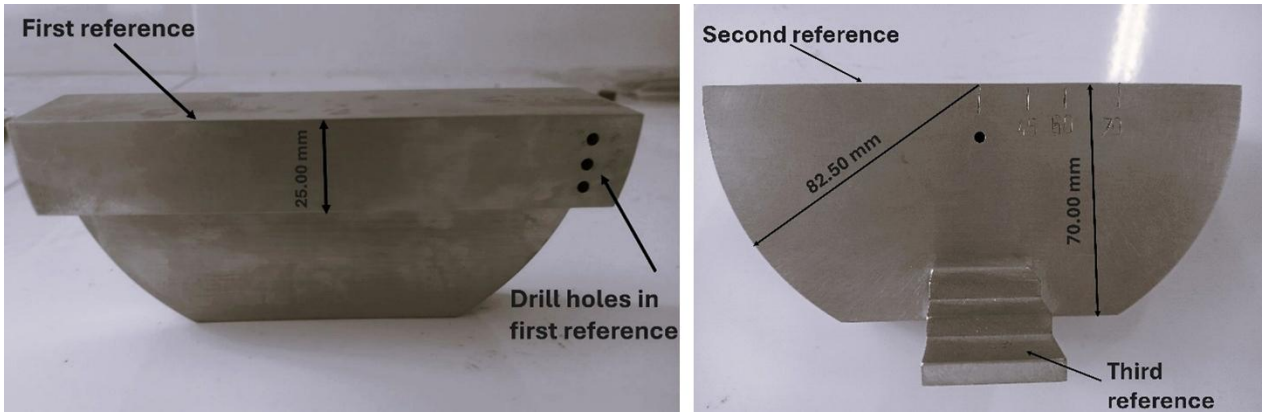

Figure 3. Standard reference block for calibration

2.2. Methods and Techniques

Acoustic measurements on the second reference were obtained using the direct contact pulse-echo technique, utilizing a Krautkrämer USM 36 ultrasonic flaw detector (General Electric) equipped with a longitudinal wave transducer. To ensure experimental repeatability and minimize uncertainty, a strict control protocol based on best practices in ultrasonic metrology was implemented [43]. All tests were conducted in a climate-controlled laboratory at a stable temperature of 24 ± 2 °C, in accordance with ASTM E494 [28], to eliminate thermal drifts that could affect propagation velocity. The use of a high-viscosity couplant (Sonotech Grade 40) was standardized to maintain constant acoustic impedance. During data acquisition, the signal maximization technique ('peaking') was applied at each measurement point; values were recorded only after the maximum amplitude had stabilized, in order to mitigate variations caused by manual pressure, following Krautkrämer's fundamentals [41]. Finally, to eliminate inter-operator error, data collection was executed entirely by a single inspector certified under ASNT (STP27016S) [44], adhering to regulatory guidelines [28, 45].

Under these controlled conditions, experimental validation was performed. Horizontal linearity (distance) calibration tests were executed operating within a frequency range of 2.25 to 5.0 MHz in a fixed position. Subsequently, to generate shear waves, mode conversion was induced by coupling the longitudinal transducer to a plexiglass angle wedge (nominal de 70°); the resulting refraction angle of 63.4° in the stainless steel was analytically validated using Snell's Law. Finally, system accuracy was verified on the block's third reference zone (stepped), recording an error of less than 0.1%, thereby confirming compliance with the tolerances of the AWS D1.6 standard [3].

The determination of ultrasonic propagation velocity (m/s), for both longitudinal and shear waves, was performed by applying Equation 4 [46]. In this expression, the time-of-flight ΔT (s) is defined as the time difference between two consecutive backwall echoes visualized on the A-Scan, obtained across the known thickness X (m) of the second reference zone. Three independent repetitions were executed for each frequency configuration and wave mode. This sampling strategy is justified by the high microstructural homogeneity achieved through the prior solution annealing treatment and the strict dimensional tolerance of the machining process, factors which minimize experimental scatter.

$$V = 2X/t \quad (4)$$

The quantification of energy losses, resulting from material attenuation and beam divergence, was performed by estimating the attenuation coefficient α (dB/mm)) using Equation 5, a formulation widely validated in the specialized literature [46–48]. Experimentally, amplitude reduction was determined via direct reading on the A-Scan display. In this context, A_0 and A correspond to the peak amplitudes of the first and second backwall echoes, respectively, acquired within the block's second reference zone for an acoustic path distance X (mm).

$$\alpha = \frac{20\, log\left({}^{A_0}/_{A}\right)}{2X} \tag{5}$$

The construction of the Distance-Amplitude Correction (DAC) curve was based on recording the amplitude decay of shear waves reflected by the Side-Drilled Holes (SDH) arranged within the block's second reference zone. The procedure commenced by coupling the transducer and maximizing the signal from the reflector closest to the beam exit point; this indication was adjusted via gain controls to reach 80% of Full Screen Height (FSH). Subsequently, without modifying the gain setting, the peak amplitudes of reflectors located at greater depths were recorded. The resulting DAC curve was obtained through the interpolation of these maximum points. The flowchart of this experimental sequence is detailed in Figure 4.

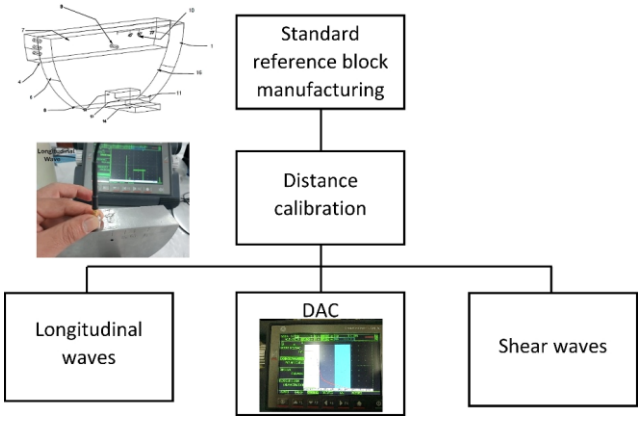

Figure 4. Experimental sequence

3. Results and Discussion

Figure 5 presents the experimental validation of the block's acoustic response in the two propagation modes critical for weld inspection. In Figure 5-a, corresponding to longitudinal waves (90°), the A-Scan reveals a sequence of sharp backwall echoes with a high Signal-to-Noise Ratio (SNR). This clean response is a direct indicator of the microstructural homogeneity achieved following heat treatment. The significant absence of structural noise or 'grass' (scattering) between the main echoes confirms that the material is free from inclusions or porosity that would attenuate the beam, validating the device for thickness metrology and vertical linearity adjustment tasks. Conversely, Figure 5-b illustrates the generation of shear waves, a mandatory requirement of the AWS D1.6 standard. The acquisition of a high-amplitude, stable signal confirms the efficacy of mode conversion at the wedge-steel interface. Physically, this demonstrates that the semi-cylindrical geometry allows the entry of the refracted beam without generating parasitic surface waves that would interfere with calibration. Furthermore, the stability of the echo validates the quality of the surface finish, the roughness of which is optimal for maintaining constant acoustic coupling and plotting reliable DAC curves in the field.

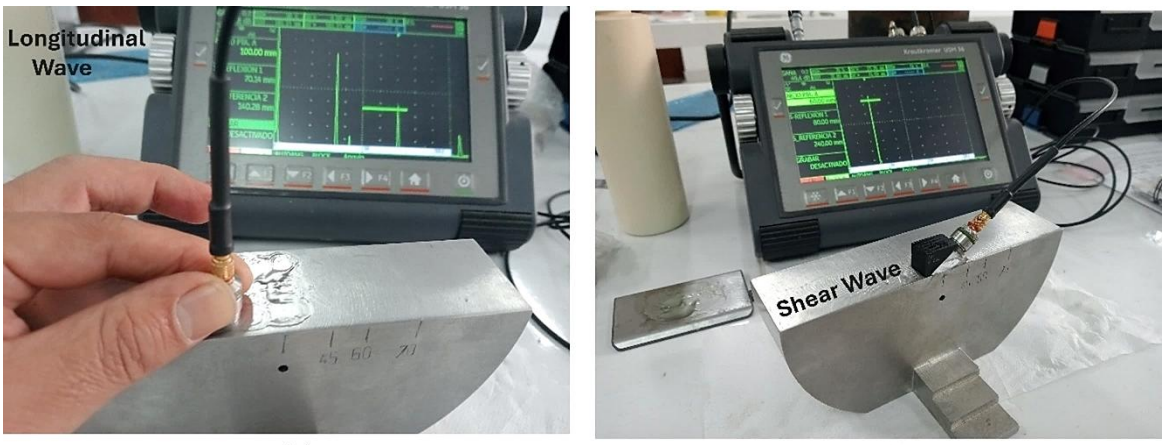

Figure 5. Distance calibration with (a) longitudinal wave and (b) shear wave

Table 1 summarizes the statistical analysis of the velocity measurements. The data reveal high experimental consistency: for longitudinal waves at 2.25 MHz, a mean of 5749 m/s was obtained with a standard deviation of merely 3.61 m/s, representing a coefficient of variation of less than 0.06%. This minimal variability confirms the macroscopic homogeneity of the base material, validating the effectiveness of the solution annealing heat treatment in mitigating local anisotropy without the need for metallographic validation. Furthermore, a slight frequency-dependent acoustic dispersion phenomenon was detected, where the shear velocity decreased from 3133 m/s (2.25 MHz) to 3100 m/s (5.0 MHz). Nevertheless, the Standard Error of the Mean (SE) remained below 8.11 m/s in all cases, confirming the precision of the method. When contrasting these results with the literature, the average experimental value (5749 ±3.6 m/s) shows notable agreement with the 5740 m/s established by Hellier [1] and Olympus standards [49] for 304 stainless steel. The relative deviation, being less than 0.2%, places the block within engineering tolerance ranges, while the shear velocity aligns perfectly with the interval (3100–3150 m/s) reported by Rawicki et al. [17] for austenitic structures.

Table 1. Acoustic velocity measurements

WAVE	Frequency (MHz)	V_1 (m/s)	V_2 (m/s)	V_3 (m/s)	Mean	Standard Deviation	SE of mean
Longitudinal	2.25	5750	5752	5745	5749	3.61	2.10
	5.0	5719	5703	5691	5704	14.05	8.11
Shear	2.25	3125	3142	3132	3133	8.54	4.93
	5.0	3097	3106	3097	3100	5.20	3.00

Table 2 presents the characterization of the ultrasonic attenuation coefficient (α), a determinant parameter for sensitivity correction in DAC curves. The data reveal a clear frequency dependence: for longitudinal waves (α_L), the coefficient increased from 0.1763 dB/mm to 0.1906 dB/mm when raising the frequency from 2.25 to 5.0 MHz. This non-linear behavior is consistent with the theoretical mechanisms of grain boundary scattering predominant in austenitic steels. A critical finding is the stability in shear wave measurements, where the standard deviation was practically negligible (0.0004 dB/mm) across the entire evaluated spectrum. The standard error of the mean (0.0003) empirically validates that the block's semi-cylindrical geometry optimizes contact, guaranteeing highly repeatable energy transfer and minimizing coupling uncertainty. Comparatively, the obtained values (0.1906 dB/mm at 5 MHz) agree with the range of 0.15–0.25 dB/mm reported by Wan et al. [23] and Moghanizadeh & Farzi [24] for medium-grain stainless steels. This agreement confirms that the block faithfully reproduces the attenuation and spectral filtering characteristics of actual welds, ratifying its suitability as a representative reference standard.

Table 2. Acoustic attenuation measurements

Wave	Frequency (MHz)	α_L (dB/mm)	α_L (dB/mm)	α_L (dB/mm)	Mean	Standard Deviation	SE of mean
Longitudinal	2.25	0.175	0.178	0.1760	0.1763	0.0015	0.0001
	5.0	0.2016	0.1820	0.1883	0.1906	0.0100	0.0057
Shear	2.25	0.0204	0.0209	0.0213	0.0209	0.0004	0.0003
	5.0	0.0225	0.0228	0.0234	0.0229	0.0004	0.0003

Figure 6 illustrates the dependence of propagation velocity on nominal frequency (2.25 MHz and 5.0 MHz) for longitudinal (a) and shear (b) waves. A decreasing trend in phase velocity is observed as frequency increases. From a physical perspective, this behavior corroborates the theory of scattering by stochastic scatterers in polycrystalline materials [26, 27, 50]: at shorter wavelengths (higher frequencies), the interaction with grain boundaries intensifies, reducing the phase velocity. However, given that this variation is less than 1%, it is concluded that the material behaves as a quasi-nondispersive medium within the operating frequency range of the AWS standard. This guarantees calibration stability regardless of the transducer employed. Furthermore, the small magnitude of the error bars (standard deviation) confirms the high repeatability of the readings, validating both the macroscopic homogeneity of the block and the quality of the surface coupling achieved.

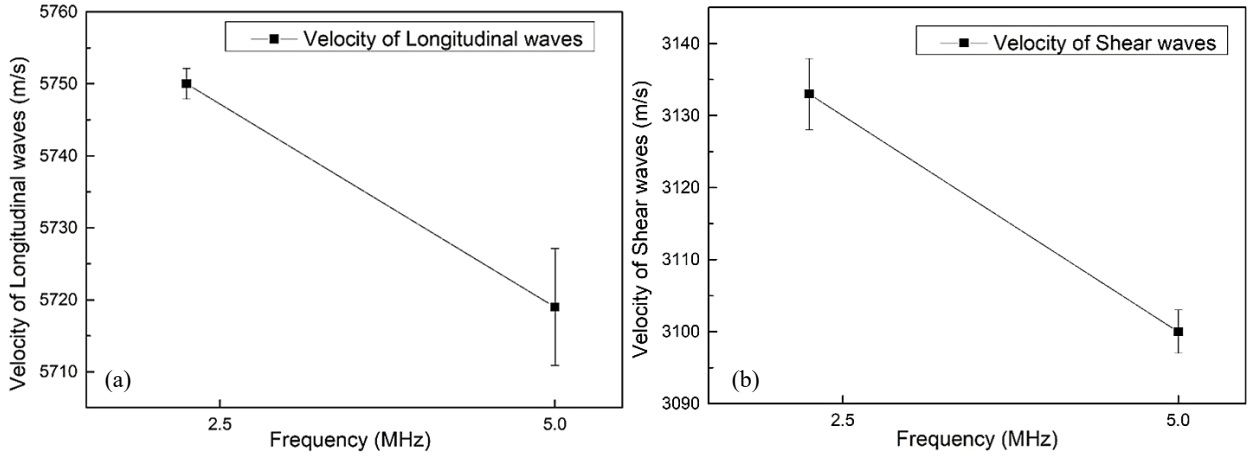

Figure 6. Ultrasonic beam velocity with (a) longitudinal wave and (b) shear wave

Figure 7 illustrates the dependence of the attenuation coefficient on frequency for longitudinal (a) and shear (b) waves. A clear positive correlation is evident: upon raising the frequency from 2.25 to 5.0 MHz, attenuation increases significantly in both modes. From the perspective of ultrasound physics, this phenomenon is attributable to scattering mechanisms at grain boundaries, operating at the transition between the Rayleigh and stochastic regimes. As the wavelength decreases at higher frequencies, it approaches the average grain size of the austenitic microstructure, intensifying energy scattering. These results corroborate the non-linear trend experimentally reported by Xu et al. [18] for welds of this type. More importantly, when contrasting these findings with studies based on simplified FEM simulations [30-32], this work provides robust empirical evidence confirming the block's ability to faithfully reproduce the actual attenuative behavior of welded components. On the other hand, it is observed that the error bars for longitudinal waves at 5.0 MHz are wider than at 2.25 MHz. This variability reflects the higher frequency beam's increased sensitivity to local microstructural heterogeneities. Nevertheless, the absolute attenuation values remain within engineering limits. In particular, the low attenuation recorded for shear waves validates the acoustic permeability of the base material, ensuring the Signal-to-Noise Ratio necessary for the precise construction of DAC curves.

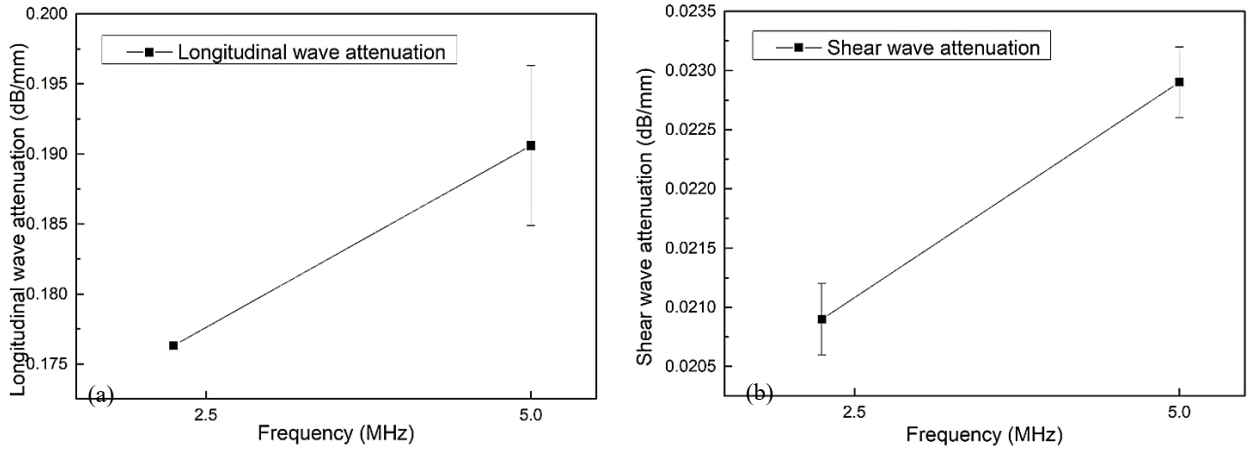

Figure 7. Attenuation coefficient with (a) longitudinal wave and (b) shear wave

From a statistical perspective, given the standard deviation observed in preliminary measurements, it was determined that a sample size of n=3 was sufficient to characterize the block's repeatability and stability, as increasing the number of repetitions would not significantly reduce the mean's confidence interval. Furthermore, the influence of frequency on acoustic properties was evaluated using a one-way Analysis of Variance (ANOVA), processed in IBM SPSS Statistics; these results are detailed in Tables 3 and 4. The analysis revealed statistically significant differences in velocity and attenuation coefficient when varying the frequency, yielding in all cases a probability value (p-value) of less than 0.05. This confirms that, at a 95% confidence level, the material's acoustic response is dependent on the transducer's operating frequency.

Table 3. ANOVA[a] for speed measures

Model		Sum of squares	gl	Mean square	F	Sig.
V_L	Regression	2992.67	1	2992.67	28.46	0.006 [b]
	Residual	420.67	4	105.12		
$V_{T63.4}$	Regression	1633.50	1	1633.50	32.67	0.005 [b]
	Residual	200.00	4	50.00		

a. Dependent variable: speed (m/s); b. Predictor variables: (Constant), probe frequency (MHz).

Table 4. ANOVA[a] for attenuation coefficient measures

Model		Sum of squares	gl	Mean square	F	Sig.
αL	Regression	0.000	1	0.000	5.98	0.07 [b]
	Residual	0.000	4	0.000		
$\alpha_{T63.4}$	Regression	0.000	1	0.000	30.01	0.005 [b]
	Residual	0.000	4	0.000		

a. Dependent variable: attenuation coefficient (dB/mm); b. Predictor variables: (Constant), probe frequency (MHz).

Additionally, the Pearson correlation coefficient corroborated a significant association between transducer frequency and acoustic parameters ($p < 0.05$). To validate the adequacy of the statistical model, Figure 8 presents the Normal Probability Plot of the residuals. The alignment of data points along the straight diagonal confirms compliance with the assumption of normality. The absence of significant deviations or skewness patterns leads to the conclusion that the variations observed in Figures 6 and 7 are attributable to the natural (random) variability of the measurement process, rather than to systematic manufacturing errors or defects in transducer coupling.

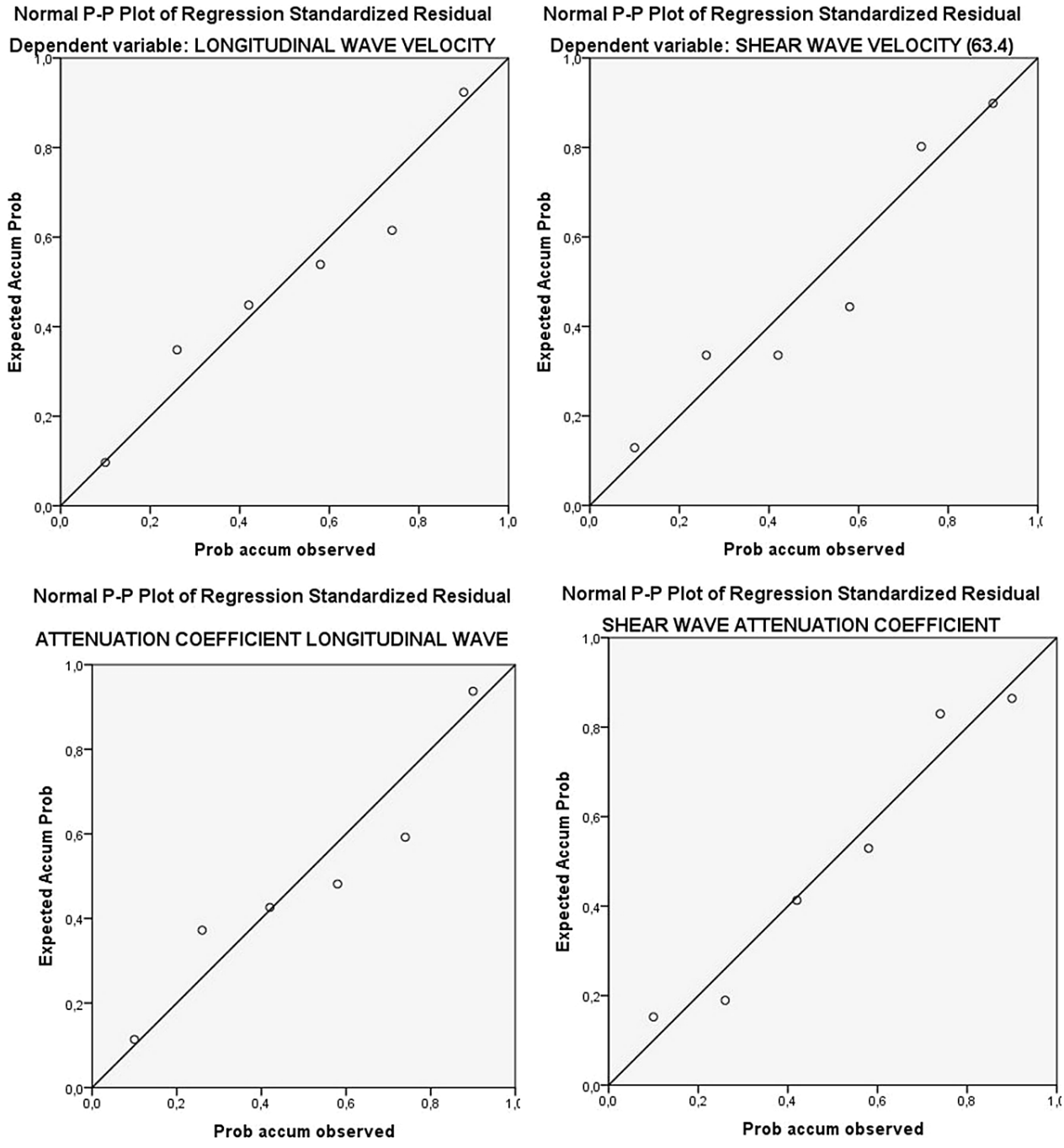

Figure 8. Normal probability for residuals

Figure 9 illustrates the successful generation of the Distance-Amplitude Correction (DAC) curve, utilizing the block's Side-Drilled Holes (SDH) zone. The procedure consisted of capturing the peak response of the three stepped cylindrical reflectors using the angle beam transducer. This geometric arrangement allows for sweeping the entire acoustic range of interest in a single setup, offering a significant operational advantage over conventional prismatic blocks that require multiple couplings. The precision achieved in plotting the curve validates compliance with the sensitivity requirements of the AWS D1.6 standard [3], allowing the inspector to effectively compensate for material attenuation and normalize rejection criteria for defects located at different depth.

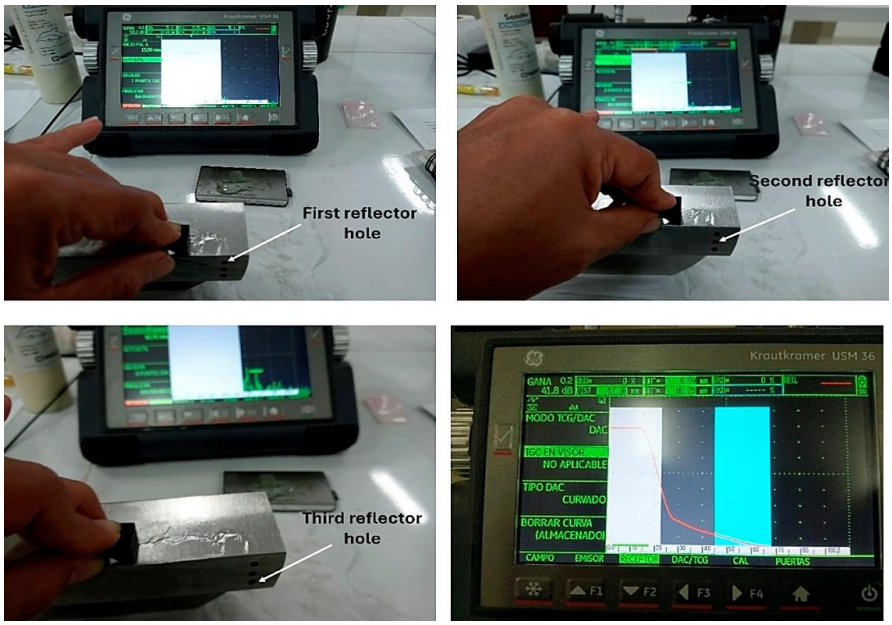

Figure 9. Experimental procedure developed to prepare the DAC curve

Figure 10 presents the in situ validation of the calibrated system applied to the inspection of a V-groove butt weld. This test confirms the successful transfer of reference parameters from the semi-cylindrical block to a real test specimen. The upper images document the manual scanning process, demonstrating on the equipment display (top right) the correct overlay of the DAC curve onto the material's background noise. In the lower panels, the detection of a specific discontinuity is detailed using a 70° angle beam transducer. The sharpness of the signal and the precision of the evaluation gate positioning demonstrate that the block provides the axial resolution and sensitivity required to discriminate between relevant indications and spurious geometric signals. This definitively validates the device's utility for Quality Assurance in industrial environments under AWS standards.

Figure 10. Inspection and evaluation procedure for discontinuities using the reference point comparison method

This study comprehensively validates the technical feasibility of the proposed reference block, demonstrating acoustic performance equivalent or superior to the standards cited in Olympus standards-NDT [49]. The results confirm that velocity and attenuation in stainless steel are strongly frequency-dependent parameters; therefore, the block's capability to reproduce this dispersive response is critical. This underscores the mandatory requirement of maintaining consistency between the calibration and inspection transducers to ensure precision in defect sizing. In terms of design innovation, the primary technical differentiation from conventional AWS blocks (such as the IIW or DSC types) lies in its functional consolidation. While traditional reference standards require multiple repositioning steps or auxiliary blocks to meet the requirements of the AWS D1.6 standard, the semi-cylindrical design integrates sensitivity, resolution, and linearity within a unified geometry. Specifically, the stepped arrangement of the Side-Drilled Holes (SDH) enables the efficient generation of multi-point DAC curves in a single scan, significantly optimizing ergonomics and operational time compared to the limitations of standard prismatic blocks.

4. Conclusion

This research comprehensively validated the technical functionality of the semi-cylindrical standard reference block (UNT patent), establishing it as a reliable tool for the ultrasonic inspection of stainless-steel welded joints. It was demonstrated that its innovative geometric configuration allows for the effective performance of distance and sensitivity calibration, strictly complying with the resolution criteria of the AWS D1.6 code. Specifically, the integration of three stepped holes proved highly effective for the immediate construction of DAC curves, eliminating the logistical complexity of employing multiple reference blocks. Field tests confirmed that the curved design facilitates optimal acoustic coupling for both longitudinal and shear waves, achieving signal clarity equivalent to international standards.

From a phenomenological perspective, the study concludes that there is a significant dependence of acoustic properties on frequency. Statistical analyses (ANOVA and Pearson) confirmed that phase velocity and attenuation vary systematically between 2.25 MHz and 5.0 MHz, evidencing the acoustic dispersion inherent to the steel microstructure. Nevertheless, the low magnitude of the standard errors validates the device's macroscopic homogeneity and manufacturing quality. Consequently, it is technically recommended to maintain frequency consistency between calibration and inspection. In summary, this block not only optimizes operational efficiency but also constitutes a robust technological reference for industrial Quality Assurance.

5. Declarations

5.1. Author Contributions

Conceptualization, J.V.; methodology, J.V., L.C., and M.T.; validation, J.V. and L.A.; formal analysis, L.C. and B.B.; investigation, L.C., L.A., and B.B.; resources, J.V. and E.A.; data curation, J.V. and M.T.; writing—original draft preparation, J.V.; writing—review and editing, L.C. and M.T.; supervision, J.V. All authors have read and agreed to the published version of the manuscript.

5.2. Data Availability Statement

The data presented in this study are available on request from the corresponding author.

5.3. Funding

The authors received no financial support for the research, authorship, and/or publication of this article.

5.4. Acknowledgments

The authors express their gratitude to the National University of Trujillo for the support provided through the Non-Destructive Testing Laboratory, where the experimental work was conducted.

5.5. Conflicts of Interest

The authors declare no conflict of interest.

6. References

[1] Hellier, C. (2013). Handbook of Nondestructive Evaluation (2nd Ed.). McGraw-Hill Education, Columbus, United States.

[2] Kot, P., Muradov, M., Gkantou, M., Kamaris, G. S., Hashim, K., & Yeboah, D. (2021). Recent advancements in non-destructive testing techniques for structural health monitoring. Applied Sciences (Switzerland), 11(6), 2750. doi:10.3390/app11062750.

[3] AWS D1.6. (2017). Structural Welding Code-Stainless Steel. American Welding Society (AWS), Miami, United States.

[4] Nguyen, P.-C., Tran, T.-T., Nguyen, H.-P., & Tran, T.-D. (2025). Nonlinear Inelastic Local Buckling Behavior of Steel Columns Subjected to Axial Compression. Civil Engineering Journal, 11(9), 3916–3933. doi:10.28991/CEJ-2025-011-09-022.

[5] Kulbayev, B., Lapin, V., Shakhnovich, A., Shokbarov, Y., Tuleyev, T., Aldakhov, S., Aldakhov, Y., & Ali, A. (2024). Strength and Deformability of Structural Steel for Use in Construction. Civil Engineering Journal (Iran), 10(3), 796–807. doi:10.28991/CEJ-2024-010-03-09.

[6] Baddoo, N. R. (2008). Stainless steel in construction: A review of research, applications, challenges and opportunities. Journal of Constructional Steel Research, 64(11), 1199–1206. doi:10.1016/j.jcsr.2008.07.011.

[7] Li, K., Zeng, J., Tang, L., Sørensen, H. E., Castro Borges, P., Geiker, M. R., Pedersen, M. T., Zhang, P., Surana, S., Maddalena, R., Wang, J., Andrade, C., Baroghel-Bouny, V., Martirena-Hernández, F., Geng, G., Kovler, K., & Wang, S. (2022). Long-term field exposure of structural concretes in marine environment: state-of-the-art review by RILEM TC 289-DCM. Materials and Structures/Materiaux et Constructions, 55(7), 205. doi:10.1617/s11527-022-02027-2.

[8] Cashell, K. A., & Baddoo, N. R. (2014). Ferritic stainless steels in structural applications. Thin-Walled Structures, 83, 169–181. doi:10.1016/j.tws.2014.03.014.

[9] Liu, M. (2022). Ultrasonic Inspection and Defect Identification of Thin - Walled Stainless Steel Welded Pipe Weld. 2022 9th International Forum on Electrical Engineering and Automation (IFEEA), 995–998. doi:10.1109/IFEEA57288.2022.10037864.

[10] Gonchar, A. V., Klyushnikov, V. A., Mishakin, V. V., & Anosov, M. S. (2021). Ultrasonic and Eddy-Current Fatigue Monitoring of Austenitic Steel Welded Joints. Russian Journal of Nondestructive Testing, 57(7), 570–578. doi:10.1134/S106183092107007X.

[11] Hou, H., Lu, D., Zhang, S., Zhang, Y., & Cheng, C. (2021). Research on on-line ultrasonic testing of small diameter thin wall stainless steel straight welded pipe. Journal of Physics: Conference Series, 1820(1), 012086. doi:10.1088/1742-6596/1820/1/012086.

[12] Vera, J., Caballero, L., & Taboada, M. (2025). Acoustic Measurements as a Nonconventional Alternative for Metallurgical Characterization of a Low-Carbon Mechanical Construction Steel. Russian Journal of Nondestructive Testing, 61(1), 32–43. doi:10.1134/S1061830924602046.

[13] Singh, R. (2020). Applied Welding Engineering: Processes, Codes, and Standards (3rd Ed.). Butterworth-Heinemann, Oxford, United Kingdom. doi:10.1016/C2019-0-03490-5.

[14] Zhang, Y., Qin, Z., Luo, S., Hyunjo, J., & Zhang, S. (2022). Design and Application of Partial Immersion Focused Ultrasonic Transducers for Austenitic Weld Inspection. Sensors, 22(7), 2671. doi:10.3390/s22072671.

[15] Verma, J., & Taiwade, R. V. (2017). Effect of welding processes and conditions on the microstructure, mechanical properties and corrosion resistance of duplex stainless-steel weldments—A review. Journal of Manufacturing Processes, 25, 134–152. doi:10.1016/j.jmapro.2016.11.003.

[16] ASTM E127-20. (2021). Standard Practice for Fabrication and Control of Flat-Bottomed Hole Ultrasonic Standard Reference Blocks. ASTM International, Pennsylvania, United States. doi:10.1520/E0127-20.

[17] Rawicki, Ł., Krawczyk, R., Słania, J., Peruń, G., Golański, G., & Łuczak, K. (2024). Analysis of the Suitability of Ultrasonic Testing for Verification of Nonuniform Welded Joints of Austenitic–Ferritic Sheets. Materials, 17(17), 4216. doi:10.3390/ma17174216.

[18] Xu, W., Li, X., Zhang, J., Xue, Z., & Cao, J. (2021). Ultrasonic signal enhancement for coarse grain materials by machine learning analysis. Ultrasonics, 117, 106550. doi:10.1016/j.ultras.2021.106550.

[19] ISO 2400:2012. (2012). Non-destructive testing—Ultrasonic testing—Specification for calibration block No. 1. International Organization for Standardization (ISO), Geneva, Switzerland.

[20] ASTM E1158-98. (2017). Standard Guide for Material Selection and Fabrication of Reference Blocks for the Pulsed Longitudinal Wave Ultrasonic Examination of Metal and Metal Alloy Production Material. ASTM International, Pennsylvania, United States. doi:10.1520/E1158-98.

[21] Dixon, S., Burrows, S. E., Dutton, B., & Fan, Y. (2011). Detection of cracks in metal sheets using pulsed laser generated ultrasound and EMAT detection. Ultrasonics, 51(1), 7–16. doi:10.1016/j.ultras.2010.05.002.

[22] Toozandehjani, M., Matori, K. A., Ostovan, F., Mustapha, F., Zahari, N. I., & Oskoueian, A. (2015). On the correlation between microstructural evolution and ultrasonic properties: a review. Journal of Materials Science, 50(7), 2643–2665. doi:10.1007/s10853-015-8855-x.

[23] Wan, T., Naoe, T., Wakui, T., Futakawa, M., Obayashi, H., & Sasa, T. (2017). Effects of grain size on ultrasonic attenuation in type 316L stainless steel. Materials, 10(7), 753. doi:10.3390/ma10070753.

[24] Moghanizadeh, A., & Farzi, A. (2016). Effect of heat treatment on an AISI 304 austenitic stainless steel evaluated by the ultrasonic attenuation coefficient. Materialpruefung/Materials Testing, 58(5), 448–452. doi:10.3139/120.110878.

[25] Tehrani, N. N., Abbasi, Z., Ozevin, D., & Indacochea, J. E. (2019). Metallurgical Characterization of a Low Carbon Steel Microstructure Using Linear and Nonlinear Ultrasonics. Journal of Materials Engineering and Performance, 28(12), 7206–7212. doi:10.1007/s11665-019-04434-z.

[26] Hakan Gür, C., & Tuncer, B. O. (2005). Characterization of microstructural phases of steels by sound velocity measurement. Materials Characterization, 55(2), 160–166. doi:10.1016/j.matchar.2005.05.002.

[27] Gür, C. H., & Çam, I. (2007). Comparison of magnetic Barkhausen noise and ultrasonic velocity measurements for microstructure evaluation of SAE 1040 and SAE 4140 steels. Materials Characterization, 58(5), 447–454. doi:10.1016/j.matchar.2006.06.008.

[28] ASTM E494-20. (2025). Standard Practice for Measuring Ultrasonic Velocity in Materials by Comparative Pulse-Echo Method. ASTM International, Pennsylvania, United States. doi:10.1520/E0494-20.

[29] Alqurashi, I., Alver, N., Bagci, U., & Catbas, F. N. (2025). A Review of Ultrasonic Testing and Evaluation Methods with Applications in Civil NDT/E. Journal of Nondestructive Evaluation, 44(2), 53. doi:10.1007/s10921-025-01190-0.

[30] Yang, C., Kaynardag, K., & Salamone, S. (2024). Investigation of wave propagation and attenuation in periodic supported rails using wave finite element method. Acta Mechanica, 235(3), 1453–1469. doi:10.1007/s00707-023-03484-8.

[31] West, G., Haslinger, S., Bamber, J., Lowe, M., Huthwaite, P., & Harris, E. (2024). Simulation of ultrasound backscatter coefficient measurement using the finite element method. Ultrasonics, 143, 107394. doi:10.1016/j.ultras.2024.107394.

[32] Schäfer, M. W., & Fischer, S. C. L. (2024). Modular, Physically Motivated Simulation Model of an Ultrasonic Testing System. Ndt, 2(3), 330–346. doi:10.3390/ndt2030020.

[33] Keuler, S., Jüngert, A., Werz, M., & Weihe, S. (2025). Influence and Potential of Additive Manufactured Reference Geometries for Ultrasonic Testing. Journal of Manufacturing and Materials Processing, 9(7), 224. doi:10.3390/jmmp9070224.

[34] Ebert, L., Jüngert, A., Sewalski, S., Werz, M., & Weihe, S. (2025). Non-destructive ultrasonic evaluation and metallographic validation of artificial defects in L-PBF additive manufactured specimens using CAD-seeding. Additive Manufacturing, 110, 104933. doi:10.1016/j.addma.2025.104933.

[35] Kim, Y. L., Cho, S., & Park, I. K. (2021). Analysis of flaw detection sensitivity of phased array ultrasonics in austenitic steel welds according to inspection conditions. Sensors (Switzerland), 21(1), 1–16. doi:10.3390/s21010242.

[36] Maharani, R. N., Mukhmad, A. F. H., Mangestiyono, W., Sutrisno, & Maulana, G. (2025). Analysis of Variables Affecting Reference Block Equivalency Process Using Ndt Ultrasonic Method†. Engineering Proceedings, 84(1), 32. doi:10.3390/engproc2025084032.

[37] Li, W., Zhang, W., Yang, G., & Chen, G. (2024). Application research on ultrasonic phased array detection algorithm for austenitic stainless steel with V-groove weld. Measurement, 226, 114169. doi:10.1016/j.measurement.2024.114169.

[38] Vera, J. (2021). Patent PE20210700Z - EMI-cylindrical calibration block for ultrasonic testing with a geometric arrangement of three references. (In Spanish).

[39] Silk, M. G. (1983). Ultrasonic transducers for nondestructive testing. Adam Hilger, Bristol, United Kingdom.

[40] ISO 16811:20102. (2012). Non-destructive testing — Ultrasonic testing — Sensitivity and range setting. International Organization for Standardization (ISO), Geneva, Switzerland.

[41] Krautkrämer, J., & Krautkrämer, H. (1990). Ultrasonic Testing of Materials. Springer, Berlin, Germany. doi:10.1007/978-3-662-10680-8.

[42] ASTM E1065/E1065M-20. (2025). Standard Practice for Evaluating Characteristics of Ultrasonic Search Units. ASTM Standard, Pennsylvania, United States. doi:10.1520/E1065_E1065M-20.

[43] ASTM E1316-20. (2020). Standard Terminology for Nondestructive Examinations. ASTM Standard, Pennsylvania, United States. doi:10.1520/E1316-20.

[44] STP27016S. (1977). ASNT Recommended Practice for Nondestructive Testing Personnel Qualification and Certification (SNT-TC-1A) and Its Use. ASTM Standard, Pennsylvania, United States. doi:10.1520/STP27016S.

[45] ASTM E664-93(2000). (2017). Standard Practice for the Measurement of the Apparent Attenuation of Longitudinal Ultrasonic Waves by Immersion Method. ASTM Standard, Pennsylvania, United States. doi:10.1520/E0664-93R00.

[46] Vijayalakshmi, K., Muthupandi, V., & Jayachitra, R. (2011). Influence of heat treatment on the microstructure, ultrasonic attenuation and hardness of SAF 2205 duplex stainless steel. Materials Science and Engineering: A, 529(1), 447–451. doi:10.1016/j.msea.2011.09.059.

[47] Stella, J., Cerezo, J., & Rodríguez, E. (2009). Characterization of the sensitization degree in the AISI 304 stainless steel using spectral analysis and conventional ultrasonic techniques. NDT & E International, 42(4), 267–274. doi:10.1016/j.ndteint.2008.11.005.

[48] de Araújo Freitas, V. L., Normando, P. G., De Albuquerque, V. H. C., De MacEdo Silva, E., Silva, A. A., & Tavares, J. M. R. S. (2011). Nondestructive characterization and evaluation of embrittlement kinetics and elastic constants of duplex stainless steel SAF 2205 for different aging times at 425°C and 475°C. Journal of Nondestructive Evaluation, 30(3), 130–136. doi:10.1007/s10921-011-0100-1.

[49] Olympus NDT. (2019). Ultrasonic Transducers Technical Notes: Material Sound Velocities. Waltham. Olympus Scientific Solutions Americas Corp, Waltham, United States.

[50] Palanichamy, P., Joseph, A., Jayakumar, T., & Raj, B. (1995). Ultrasonic velocity measurements for estimation of grain size in austenitic stainless steel. NDT and E International, 28(3), 179–185. doi:10.1016/0963-8695(95)00011-L.